Charge and spin structures in the one-dimensional t-J model

F. F. Assaad and D. Würtz
Interdisziplinäres Projektzentrum für Supercomputing, ETH Zürich, Switzerland and Institute for Theoretical Physics, ETH Zürich, Hönggerberg, Switzerland
(Received 28 September 1990; revised manuscript received 11 March 1991)

The physics of the one-dimensional t-J model may be determined at $J/t \to 0$ (i.e., the $U/t \to \infty$ limit of the repulsive Hubbard model) and at $J/t = 2$ with the use of the Bethe ansatz. To get a full understanding of the charge and spin correlation functions for all values of J/t, one has to resort to numerical methods. We have used two numerical methods (the world-line quantum Monte Carlo algorithm and the quantum transfer-matrix algorithm) to get information on charge and spin static structure factors, pairing correlations, and critical exponents. The $(1+1)$-dimensional classical system corresponding to the one-dimensional t-J model, on which the Monte Carlo technique is used, is identified to a fifteen-vertex model. We show that the t-J model undergoes phase separation at large values of J/t. Before phase separation, both critical exponents and pairing correlations in the extended s-wave channel favor the onset of superconductivity. For low values of J/t, the model shows a $U/t \to \infty$ Hubbard-like character.

I. INTRODUCTION

The t-J model provides one of the most interesting and simplest models to study the physics of doped antiferromagnets. The interest in this model was stimulated by Anderson's[1] suggestion that it contains the relevant physics of the copper oxide planes in high-T_c superconducting materials. Furthermore, Zhang and Rice[2] derived the t-J model from a multiband Hubbard model describing the copper oxide planes. The t-J model that we have considered reads

$$H = -t \sum_{\langle i,j \rangle, \sigma} [(1-n_{i,-\sigma}) c^{\dagger}_{i,\sigma} c_{j,\sigma} (1-n_{j,-\sigma}) + \text{H.c.}] + J \sum_{\langle i,j \rangle} (\mathbf{S}_i \cdot \mathbf{S}_j - \tfrac{1}{4} n_i n_j) \ . \quad (1)$$

Here $\langle i,j \rangle$ denotes the sum over next neighbors, $c^{\dagger}_{i,\sigma}$ creates an electron on site i with z component of spin σ, $n_{i,\sigma} = c^{\dagger}_{i,\sigma} c_{i,\sigma}$, and $\mathbf{S}_i$ is the spin operator at site i. Electrons on the lattice are thus submitted to a next-nearest Heisenberg interaction (which favors antiferromagnetic alignment of spins) and are allowed to hop between adjacent sites. Since double occupancy is prohibited, the model reduces to the Heisenberg Hamiltonian in the special case of one electron per site (i.e., half band filling). Furthermore, at $J = 4t^2/U$, the t-J model is an approximate effective Hamiltonian for the large-(U/t) limit of the Hubbard model.[3] Clearly, the key question in two dimensions is to establish if the t-J model may explain the unusual normal state as well as superconducting state properties of the copper oxide planes in high-T_c materials.

Besides the interest of modeling the two-dimensional copper oxide planes, the one-dimensional counterpart of the t-J model has fascinated many researchers since it shows a very rich phase diagram. In one dimension, the Hubbard model may be solved exactly by means of the Bethe ansatz.[4] It has been shown numerically, and recently analytically, that the repulsive Hubbard model scales to the Tomonaga-Luttinger model.[5-8] The provides information on the t-J model in the limit $J/t \to 0$. In the supersymmetric case $J/t = 2$, the t-J model may equally be solved with a Bethe ansatz.[9-11] From the Bethe ansatz solution, the critical exponents can be calculated.[12] This calculation shows that the t-J model at $J/t = 2$ belongs to the same universality class as that of the repulsive Hubbard model. $J/t = 2$ and $J/t \to 0$ are the two points in parameter space where analytical results are available. In order to get a complete picture of the phase diagram, one has to make use of numerical methods. Our numerical investigation is based on two methods: the quantum Monte Carlo world-line algorithm[13,14] (WLA) and the quantum transfer-matrix algorithm (TMA).[15-17] Both methods provide thermodynamic quantities in the canonical ensemble. The TMA produces exact results but is restricted to small lattices, whereas the WLA may deal with large lattices but yields results with statistical uncertainty. Some preliminary numerical work on the t-J model has already been carried out by Imada.[18] His results point out a very strong enhancement of the extended s-wave pairing susceptibility at low temperatures and for relatively large values of J/t. The aim of this work is to provide further understanding of the electronic structure of the t-J model as a function of the coupling J/t and the band filling ρ. The questions we wish to answer include the following: (a) At which value of J/t does the t-J model lose its large-U Hubbard character and what is the nature of the resulting ground state? (b) For which values of J/t and ρ does phase separation occur, and how does it occur? (c) What is the nature of the ground state before phase separation?

The text is organized as follows. In Sec. II, we review briefly the foundations of the WLA and TMA. Both methods rely on Suzuki's[19] generalization of the Trotter formula[20] to demonstrate that the partition function of a

d-dimensional quantum-mechanical system is equivalent to that of a $(d+1)$-dimensional classical system. We identify the $(1+1)$-dimensional classical system corresponding to the one-dimensional t-J model to a fifteen-vertex model. As in all quantum Monte Carlo procedures, there is a set of controllable approximations that one has to carry out in order to render the simulation possible. We have found it important to include a brief section on this topic.

In Sec. III, we discuss our numerical results. In order to answer the above questions, we have measured the static charge and spin structure factors as well as pairing correlations in the extended s-wave channel. We have carried out a finite-size scaling analysis of the charge and spin critical structure factors at $J/t=2.2$ and at quarter band filling so as to determine the $2k_f$ charge and spin exponents. In order to get more insight into the nature of the transition to the phase separated state, we have looked into the spinless electron model (t-V model) defined by

$$H_{t\text{-}V}=-t\sum_i (c_{i+1}^{\dagger}c_i+\text{H.c.})-V\sum_i n_{i+1}n_i \ . \tag{2}$$

Here $V>0$ so that there is an attractive density-density interaction between next neighbors. Through a Jordan-Wigner transformation, the t-V model produces the same physics as the spin model

$$H_{XXXZ}=-J_X\sum_i (S_i^+S_{i+1}^-+S_i^-S_{i+1}^+)-J_Z\sum_i S_i^zS_{i+1}^z \ , \tag{3}$$

which has been solved by means of a Bethe ansatz by Yang and Yang.[21] Furthermore, the t-V model is a Luttinger liquid.[22,23] [The equivalence follows by identifying down spins to holes. The Hamiltonian (3) may then be expressed by hard-core bosons submitted to a nearest-neighbor hopping term and a density-density interaction of magnitude $-J_Z$ between adjacent sites. On a one-dimensional lattice, this produces the same physics as the t-V model.] The t-V model shows a first-order phase transition to a phase separated state at $V/t=2$ and for all band fillings.

Finally, in Sec. IV, we summarize our results and give a qualitative phase diagram of the one-dimensional t-J model. Preliminary results of this work were already given in Ref. 24.

II. PATH-INTEGRAL FORMULATION OF THE PARTITION FUNCTION

Both the WLA and TMA (Ref. 25) rely on a path-integral formulation of the partition function. The principle advantage of those algorithms is that they allow one to simulate easily any one-dimensional quantum-mechanical model on a lattice with arbitrary next-neighbor interactions. This is not the case for *determinant methods*[18,26,27] since they require the ability of decomposing the many-body interaction into one-body operators interacting with Hubbard-Stratonovic fields. The details of both methods are well known so that we will only sketch the main ideas for the special case of the t-J model.

Following Barma and Shastry,[28] we write the t-J Hamiltonian as

$$H=\sum_i H_{i,i+1}=H_{\text{odd}}+H_{\text{even}} \ , \tag{4}$$

where

$$H_{i,i+1}=-t\sum_{\sigma}[(1-n_{i+1,-\sigma})c_{i+1,\sigma}^{\dagger}c_{i,\sigma}(1-n_{i,-\sigma})+\text{H.c.}]$$
$$+J(\mathbf{S}_{i+1}\cdot\mathbf{S}_i-\tfrac{1}{4}n_{i+1}n_i) \ ,$$
$$H_{\text{odd}}=\sum_{i\ \text{odd}} H_{i,i+1}, \quad H_{\text{even}}=\sum_{i\ \text{even}} H_{i,i+1} \ .$$

Since there are only next-neighbor interactions, the terms in the sum forming H_{odd} commute. The same holds for H_{even}. However, H_{odd} and H_{even} do not commute. The canonical partition function may then be written as

$$\begin{aligned} Z&=\text{Tr}(e^{-\beta H})=\text{Tr}[(e^{-\Delta\tau(H_{\text{odd}}+H_{\text{even}})})^M] \\ &=\text{Tr}[(e^{-\Delta\tau H_{\text{odd}}}e^{-\Delta\tau H_{\text{even}}})^M]+O((\Delta\tau)^2) \\ &=\sum_{i_1,i_2,\ldots,i_{2M}} \langle i_1|U_{\text{odd}}|i_{2M}\rangle\langle i_{2M}|U_{\text{even}}|i_{2M-1}\rangle\cdots\langle i_3|U_{\text{odd}}|i_2\rangle\langle i_2|U_{\text{even}}|i_1\rangle+O((\Delta\tau)^2) \ . \end{aligned} \tag{5}$$

Here β is the inverse temperature (or imaginary time) $\Delta\tau=\beta/M$,

$$U_{\text{odd}}=e^{-\Delta\tau H_{\text{odd}}}, \quad U_{\text{even}}=e^{-\Delta\tau H_{\text{even}}} \ ,$$

and

$$\sum_{i_k}|i_k\rangle\langle i_k|=1 \quad (k=1,2,\ldots,2M) \ .$$

The states $|i_k\rangle$ are in real space.

The state $|i_1\rangle$ thus evolves in complex time according to the imaginary-time-evolution operators U_{even} and U_{odd}. Each element of the above sum may be represented graphically on a checkerboard [see Fig. 1(a)] in terms of two kinds of world lines (black and gray) which follow the imaginary time evolution of the up and down spins. Due to the breakup of the Hamiltonian in an odd and even part, the particles may move or interact only within the shaded squares. The t-J model conserves the particle number as well as the total magnetization, so that the number of world lines of each type is conserved throughout the imaginary time propagation.

Since $H_{\text{even(odd)}}$ is a sum of commuting terms, the evaluation of the matrix element $\langle i|U_{\text{even(odd)}}|i'\rangle$ reduces to

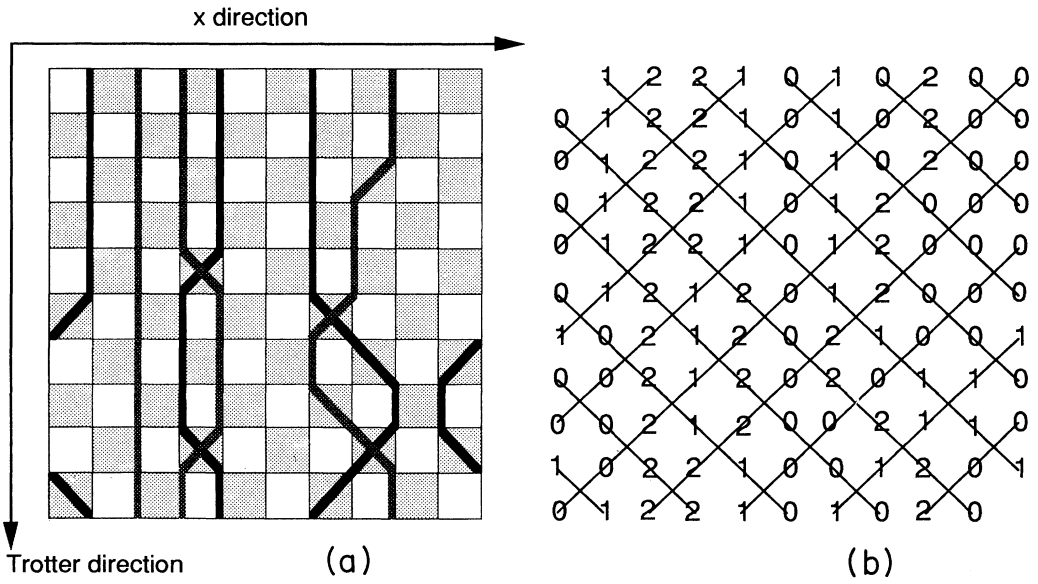

FIG. 1. (a) An example of a world-line configuration. The imaginary time (Trotter direction) runs along the vertical axis, and the real-space (x direction) along the horizontal axis. The black (gray) world line represents up (down) spins. The world lines may only move or interact within a shaded square. (b) The world-line configuration shown in (a) is drawn in terms of the 15-vertex model.

solving a two site problem. For the t-J model, the matrix elements of the two site problem follow from

$$
\begin{aligned}
&e^{-\Delta\tau H_{i,i+1}}|0,0\rangle = |0,0\rangle \ , \\
&e^{-\Delta\tau H_{i,i+1}}|\sigma,0\rangle = \cosh(\Delta\tau t)|\sigma,0\rangle + \sinh(\Delta\tau t)|0,\sigma\rangle \ , \\
&e^{-\Delta\tau H_{i,i+1}}|\sigma,\sigma\rangle = |\sigma,\sigma\rangle \ , \\
&e^{-\Delta\tau H_{i,i+1}}|\sigma,-\sigma\rangle = e^{\Delta\tau J/2}[\cosh(\Delta\tau J/2)|\sigma,-\sigma\rangle \\
&\qquad\qquad - \sinh(\Delta\tau J/2)|-\sigma,\sigma\rangle] \ .
\end{aligned}
\tag{6}
$$

Here the ket $|\ ,\ \rangle$ describes the state on sites i and $i+1$. Note that only 15 of the 81 possible matrix elements take nonzero values. They are shown in Fig. 2.

When measuring observables, one has to distinguish between observables that locally conserve charge and spin (spin and charge structure factors) and observables that globally conserve charge and spin (Green functions and pairing correlations). The energy follows its own rule since it may be decomposed in an odd and even part. It is evaluated with

$$
\begin{aligned}
\langle E\rangle = \sum_{i_1,i_2,\ldots,i_{2M}} & P(i_1,i_2,\ldots,i_{2M}) \\
& \times \left[\frac{\langle i_2|U_{\text{even}}H_{\text{even}}|i_1\rangle}{\langle i_2|U_{\text{even}}|i_1\rangle} \right. \\
& \left. + \frac{\langle i_3|U_{\text{odd}}H_{\text{odd}}|i_2\rangle}{\langle i_3|U_{\text{odd}}|i_2\rangle} \right] \\
& + O((\Delta\tau)^2) \ ,
\end{aligned}
\tag{7}
$$

where

$$
P(i_1,i_2,\ldots,i_{2M}) = \frac{\langle i_1|U_{\text{odd}}|i_{2M}\rangle \cdots \langle i_2|U_{\text{even}}|i_1\rangle}{\sum_{i_1,i_2,\ldots,i_{2M}} \langle i_1|U_{\text{odd}}|i_{2M}\rangle \cdots \langle i_2|U_{\text{even}}|i_1\rangle} \ .
$$

The spin-spin (charge-charge) correlations are estimated through

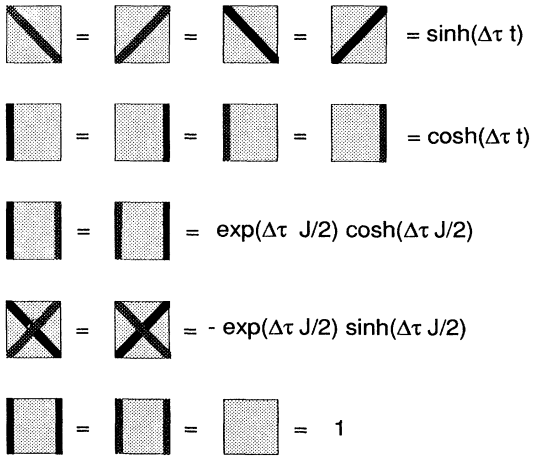

FIG. 2. The 15 matrix elements for given plaquette configurations. All other plaquette configurations have vanishing weights.

$$\langle S_i^z S_j^z \rangle = \sum_{i_1,i_2,\ldots,i_{2M}} P(i_1,i_2,\ldots,i_{2M}) \times \frac{\langle i_2|(U_{\text{even}} S_i^z S_j^z + S_i^z S_j^z U_{\text{even}})|i_1\rangle}{2\langle i_2|U_{\text{even}}|i_1\rangle} + O((\Delta\tau)^2) \ . \quad (8)$$

The above procedure may not be applied for equal-time Green functions since the quotients in Eqs. (7) and (8) would not be well defined. This difficulty may be circumvented by the use of

$$\langle c_{i,\sigma}^\dagger c_{j,\sigma} \rangle = \frac{\sum_{i_1',i_1,\ldots,i_{2M}} P(i_1',i_1,\ldots,i_{2M}) \langle i_1'|c_{i,\sigma}^\dagger c_{j,\sigma}|i_1\rangle}{\sum_{i_1',i_1,\ldots,i_{2M}} P(i_1',i_1,\ldots,i_{2M}) \langle i_1'|i_1\rangle} + O(\Delta\tau) \ , \quad (9)$$

where

$$P(i_1',i_1,\ldots,i_{2M}) = \frac{\langle i_1|U_{\text{odd}}|i_{2M}\rangle \cdots \langle i_2|U_{\text{even}}|i_1'\rangle}{\sum_{i_1',i_1,\ldots,i_{2M}} |\langle i_1|U_{\text{odd}}|i_{2M}\rangle \cdots \langle i_2|U_{\text{even}}|i_1'\rangle|} \ .$$

For equal-time Green functions a single break in the world lines is allowed. In general, the type of break allowed depends on the observable.

We may now evaluate observables by creating a set of world-line configurations according to the probability distributions $|P(i_1,i_2,\ldots,i_{2M})|$ or $|P(i_1',i_1,\ldots,i_{2M})|$ with the Monte Carlo method (WLA) or by explicitly carrying out the sum over all world-line configurations (TMA).

A. The WLA and sources of systematic errors

The Monte Carlo procedure requires the quantity $P(i_1,i_2,\ldots,i_{2M})$ to be positive since it interprets it as a probability distribution. Assuming fixed boundary conditions, one may show that although the matrix element that interchanges two spins (6) is negative, $P(i_1,i_2,\ldots,i_{2M})$ is always positive. On the other hand, $P(i_1',i_1,\ldots,i_{2M})$ may be negative, but the combined quantity $P(i_1',i_1,\ldots,i_{2M})\langle i_1'|c_{i,\sigma}^\dagger c_{j,\sigma}|i_1\rangle$ is positive. The same holds for pairing correlations. Fixed boundary conditions thus yield no minus-sign problems. The situation becomes more complicated when one uses periodic boundary conditions. In this case, a world line acquires a factor $(-1)^{N-1}$ when it crosses the boundary. Here N stands for the number of particles on the lattice. This has as a consequence that in the subspace of world-line configurations with nonzero-winding number, one may generate configurations with negative weights. However, in the subspace of zero-winding number, all configurations have positive weights. It should be emphasized that the above minus-sign problem originates from a boundary effect and is thus of different nature than the one present in the two-dimensional Hubbard model[26,27] for example. As will be discussed below, we have restricted our sampling to the subspace of zero-winding number.

We have used the moves shown in Fig. 3 to upgrade a world-line configuration. The charge move [Fig. 3(a)] on its own is used to simulate the t-V (2) model or the hopping term in the t-J model. The spin move [Fig. 3(b)] on its own will simulate a Heisenberg model. Simulating the t-J model is somewhat more complicated since combining the charge and spin moves will not yield ergodicity within a subspace of constant total magnetization. For this reason, one has to include the move shown in Fig. 3(c). The charge and spin moves [Figs. 3(a) and 3(b)] are local in the sense that they only involve the four shaded squares surrounding the unshaded square where the move is carried out. This allows one to upgrade one-quarter of the unshaded squares in parallel. Clearly, the above moves conserve the winding number. Restricting the sampling to the subspace of zero-winding configurations introduces an approximation to periodic boundary conditions. However, on a finite-size lattice, one is free to choose arbitrary boundary conditions since they will have no effect on the thermodynamic limit. In this sense, restricting the sampling to the subspace of zero-winding number may not be considered as a source of systematic errors since it just modifies the boundary conditions. Figure 4 compares the finite-size scaling of the energy of a free spinless electron gas [t-V model (2) at $V/t=0$] at finite temperature for periodic, antiperiodic, and *zero-winding* boundary conditions. Although the approach to the thermodynamic value depends on the choice of the boundary conditions, the thermodynamic value itself is

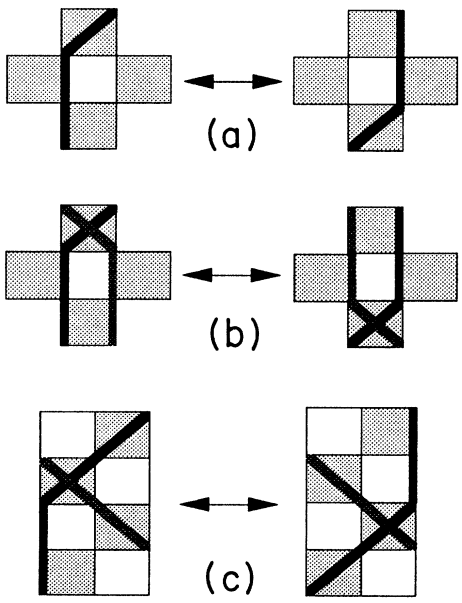

FIG. 3. Local moves used to upgrade a world-line configuration (black and gray lines may be interchanged). Only the move (a) is required to simulate free electrons or the t-V model (2). The move (b) on its own will simulate the Heisenberg chain. In order to achieve ergodicity when simulated the t-J model, one has to include move (c).

independent of the boundary conditions. Another consequence of different choices of boundary conditions is the scaling of the energy as a function of the temperature (Fig. 5). Figure 5 equally gives a measure of the effect of the winding number on small lattices as a function of the temperature. For antiperiodic boundary conditions and an even number of particles, all world-line configurations have positive weights. Thus the difference between the TMA and the WLA data consists of the sum over all nonzero-winding number world-line configurations which are omitted in the WLA.

In order to achieve ergodicity within the subspace of zero-winding world-line configurations, one has to introduce a global move which changes the color of a world line. This allows one to sample regions of different total magnetization. This move is very expensive in CPU time since it inhibits vectorization. It is thus important to delimit the parameter range where this move may be omitted without introducing systematic errors. The t-J model has an SU(2) spin symmetry so that the expectation value of the total magnetization vanishes. At temperatures where the ground-state properties dominate, the expectation value of the square of the total magnetization will also vanish provided that the ground state is a spin singlet. In those circumstances, omitting the above global move yields no source of systematic errors. Ogata and Shiba[6] have shown for the $U/t \to \infty$ Hubbard model that the ground state of a system with $4n$ (where n is an integer) electrons and periodic boundary conditions is a spin triplet. Imposing antiperiodic boundary conditions yields a spin singlet. On the other hand, systems with $4n+2$ electrons and periodic boundary conditions have a singlet ground state. This situation is present in the t-J model for values of $J/t < 2$. For values of $J/t \geq 2$ both periodic and antiperiodic boundary conditions yield a singlet ground state. As mentioned above, in the WLA one does not have true periodic or antiperiodic boundary conditions since the sampling is restricted to the subspace of zero-winding number. We have thus carried out a set of simulations at low temperatures (i.e., $\beta t \geq 15$) including the above global move. Our results show that the acceptance rate of the global move vanishes for values of $J/t \geq 2$ so that in this parameter range one may omit the global move without introducing systematic errors. For $J/t < 2$, omitting the global move introduces small systematic errors but does not change the qualitative results. Clearly, at high temperatures it is crucial to include the global move (see Fig. 5). Unless mentioned otherwise, we have restricted the sampling to the subspace of zero total magnetization.

The path-integral formulation of the partition function introduces systematic errors of the order of $\beta(\Delta\tau)^2 t^\mu J^\nu$, where μ and ν are positive (or zero) integers which satisfy $\nu+\mu=3$. This source of systematic errors is controllable since one can extrapolate to $\Delta\tau \to 0$ while keeping β and J/t constant. We have carried out simulations at

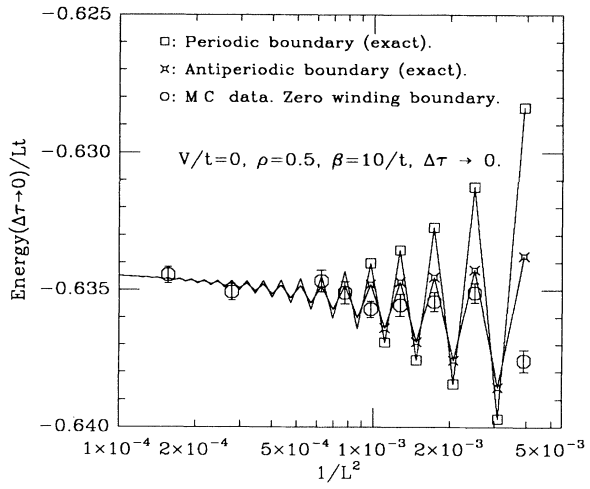

FIG. 4. Comparison between periodic, antiperiodic, and *zero-winding* boundary conditions for free spinless electron gas at quarter band filling [t-V model (2) at $V/t=0$]. The data for both periodic and antiperiodic boundary conditions were calculated exactly within the canonical ensemble whereas the data for *zero-winding* boundary conditions was calculated with the Monte Carlo (MC) method. In order to extrapolate to $\Delta\tau \to 0$ we have carried out simulations on the 80-site lattice at $\Delta\tau=0.125$, 0.25, and 0.5. The energy scaled to the form $E(\Delta\tau, L=80) = -0.6344(3) - 0.107(4)\Delta\tau^2$. For the other lattice sizes, the simulations were carried out at $\Delta\tau=0.125$. The systematic error produced by the finite value of $\Delta\tau$ was taken into account by using the same scaling form as for the $L=80$ lattice [i.e., we assumed the $\Delta\tau^2(-0.107\pm0.004)$ coefficient to be size independent].

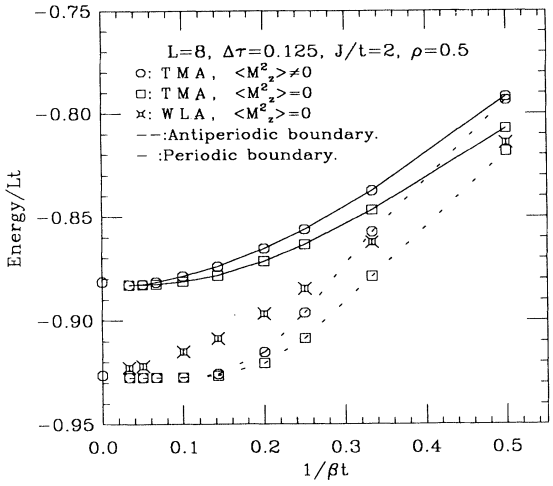

FIG. 5. Temperature dependence of the energy per site for periodic, antiperiodic and *zero-winding* boundary conditions for the t-J model. One may see that at low temperatures and at the considered value of J/t, restricting the sampling to the subspace of zero total magnetization yields no source of systematic errors. The two data points at zero temperature come from the exact diagonalization code of Ogata *et al.*[32] Comparing the WLA data and the TMA data for antiperiodic boundary conditions yields a measure of the contribution to the energy of nonzero-winding number configurations as a function of temperature (see text).

$J/t=2$, $\beta t=15$ on a 16-site lattice and at quarter band filling for $\Delta\tau=0.0625$, 0.125, 0.25, 0.375, and 0.5. We found the energy per site to scale to the form $E(\Delta\tau)=-0.9055(3)-[0.067(1)](\Delta\tau)^2$. The $\Delta\tau$ effects on the spin and charge structure factors were too small in comparison to our error bars so as to obtain reliable results. Unless mentioned otherwise, we have carried out our simulations at $\Delta\tau=0.125$. This introduces a systematic error of the order of 0.2% on the energy.

B. The transfer-matrix method

The TMA sums up all allowed world-line configurations by going through the checkerboard lattice along the imaginary time or Trotter direction. Spin configurations along the real-space direction were coded into a Cray word reserving two bits for a site and two additional bits for the boundary conditions. Periodic as well as antiperiodic boundary conditions were implemented. All symmetries including spin rotation, translation, and inflection were considered to keep the number of different configurations small. Observables were calculated through the use of Eqs. (7) and (8). It is worth noting that the energy as well as the spin and charge structure factors were measured numerically by bit manipulations, thus leading to a very efficient algorithm. The only source of systematic errors in the TMA comes from the path-integral formulation of the partition function.

C. Formulation in terms of a vertex model

Figure 1(a) shows how the one-dimensional t-J model may be mapped on the alternative two-dimensional checkerboard lattice. We introduce a new lattice formed by the diagonals going through the shaded squares and rotate it by 45°. We now label the bonds of the new lattice according to the following rules: if on a horizontal bond of the new lattice an up (down) spin is present, we label the bond with a 1 (2) and a zero otherwise. The same holds for the vertical bonds. These rules lead to a description of the one-dimensional t-J model in terms of a fifteen-vertex model [Fig. 1(b)]. The equivalent observation for the XYZ model was first made by Barma and Shastry[29] yielding the well-known eight-vertex model. From Baxter's[30] results on the eight-vertex model, one can then recover physical quantities such as the ground-state energy. However, less work has been done on fifteen-vertex models. Very recently, Gölzer[31] studied a novel fifteen-vertex solution to the Sutherland equations. It is interesting to note that in the special case $J=2t$, our vertex weights fulfill Sutherland's equations derived in Ref. 31. Further work in this direction is under progress.

III. RESULTS AND DISCUSSION

We have carried out simulations for lattice sizes ranging from $L=16$ to 32, and at three different band fillings: $\rho=0.75$, 0.5, and 0.25 ($\rho\equiv$number of particles/L). The temperatures were chosen low enough ($\beta t=15-30$) so as to get a good idea of the ground-state energy, spin structure, and charge structure. Our estimated ground-state energy as a function of the filling and at $J/t=2$ is compared in Fig. 6 to the exact solution.[11] The agreement is good.

A. Charge and spin structure factors

The static structure factors reflect the presence and nature of long-range spin and charge correlations. They are defined by the Fourier transform of the real-space correlations and may be written as

$$S_{\text{charge,spin}}(k)=\langle \hat{S}_{\text{charge,spin}}(k)\hat{S}_{\text{charge,spin}}(-k)\rangle \ , \tag{10}$$

where

$$\hat{S}_{\text{charge,spin}}(k)=\frac{1}{\sqrt{L}}\sum_q \left[c^\dagger_{q,\uparrow}c_{q+k,\uparrow}\pm c^\dagger_{q,\downarrow}c_{q+k,\downarrow}\right] .$$

In the above equation, charge (spin) is associated with the $+$ ($-$) sign. Translation invariance was imposed while measuring the above observables. The static structure factors are related to the dynamical structure factors through

$$\hat{S}_{\text{charge,spin}}(k)=\tfrac{1}{2}\int d\omega\chi_{\text{charge,spin}}(k,\omega) \ , \tag{11}$$

where the dynamical structure factors are defined by

$$\chi_{\text{charge,spin}}(k,\omega) = \frac{1}{Z}\sum_{i,j}|\langle\psi_i|\hat{S}_{\text{charge,spin}}(k)|\psi_j\rangle|^2 \times(e^{-\beta E_i}+e^{-\beta E_j})\delta(\omega-(E_j-E_i)) \ . \tag{12}$$

In the above equation, $|\psi_i\rangle$ denotes an eigenstate of the Hamiltonian with eigenvalue E_i.

As mentioned in the Introduction, the long-range behavior of the repulsive Hubbard model and of the t-J

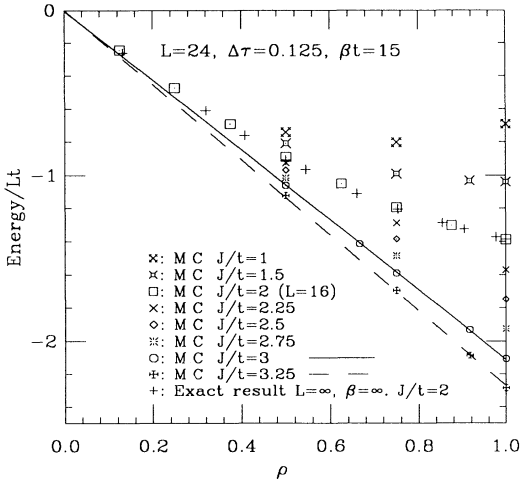

FIG. 6. Energy per site as a function of the band filling for the t-J model. J/t ranges from 1 to 3.25 and the inverse temperature is set to $\beta=15/t$. At $J/t=2$, our estimated energy (squares) is compared with the exact results of Ref. 11 (pluses). As emphasized in the plot, the energy scales almost linearly with band filling at $J/t=3$ and 3.25

model at $J/t=2$ belong to the same universality class.[7,12] The real-space correlations show a power-law decay. All critical exponents are determined by a dimensionless quantity K_ρ:

$$\langle n(r)n(0)\rangle \sim A_0 r^{-2} + A_1\cos(2k_F r) r^{-(1+K_\rho)} + A_2\cos(4k_F r) r^{-4K_\rho},$$
$$\langle S_z(r)S_z(0)\rangle \sim B_0 r^{-2} + B_1\cos(2k_F r) r^{-(1+K_\rho)}, \quad (13)$$
$$\langle b^\dagger(r)b(0)\rangle \sim C_0 r^{-(1+1/k_\rho)} + C_1\cos(2k_F r) r^{-(K_\rho+1/K_\rho)},$$

where $r \gg 1$ and $b(r)=(1/\sqrt{2})(c_{r,\uparrow}c_{r+1,\downarrow} - c_{r,\downarrow}c_{r+1,\uparrow})$.

In the above equations, we have omitted logarithmic corrections. For the $U/t \to \infty$ repulsive Hubbard model, $K_\rho=0.5$ independently of the band filling. Note that in the repulsive Hubbard model, the spin-spin correlations dominate due to the logarithmic corrections.[8] In the t-J model, $J/t=2$, K_ρ increases from $K_\rho=0.5$ to 1 as the band filling increases from $\rho=0$ to 1. From the above equations one may see that the pairing correlations dominate the long-range order provided that $K_\rho > 1$. This situation never occurs in the repulsive Hubbard model and in the t-J model at $J/t=2$.

1. *Quarter band filling ($\rho=0.5$)*

In the t-J model, the hopping term and the Heisenberg interaction term compete against each other. The hopping term alone shows a $4k_F$ ($k_F=\rho\pi/2$) charge density wave with power-law decay $\langle n_0 n_r\rangle = \rho^2 + (1/2\pi^2)[\cos(4k_F r)-1]r^{-2}$ for $r>1$. On the other hand, the Heisenberg term favors an antiferromagnetic alignment of spins on adjacent sites. The ground state at $J/t=0$ is degenerate in the spin degrees of freedom. This degeneracy is lifted by a small value of J/t and produces a $2k_F$ spin density wave. Since the t-J model reduces to the large-U limit of the Hubbard model for $J/t \ll 1$, the same charge structure and spin structure are expected.[5,6] As J/t is enhanced, one expects $S_{\text{charge}}(4k_F)$ to decrease in magnitude and $S_{\text{charge}}(2k_F)$ to increase since charges will gradually favor being on adjacent sites [Figs. 7(a) and

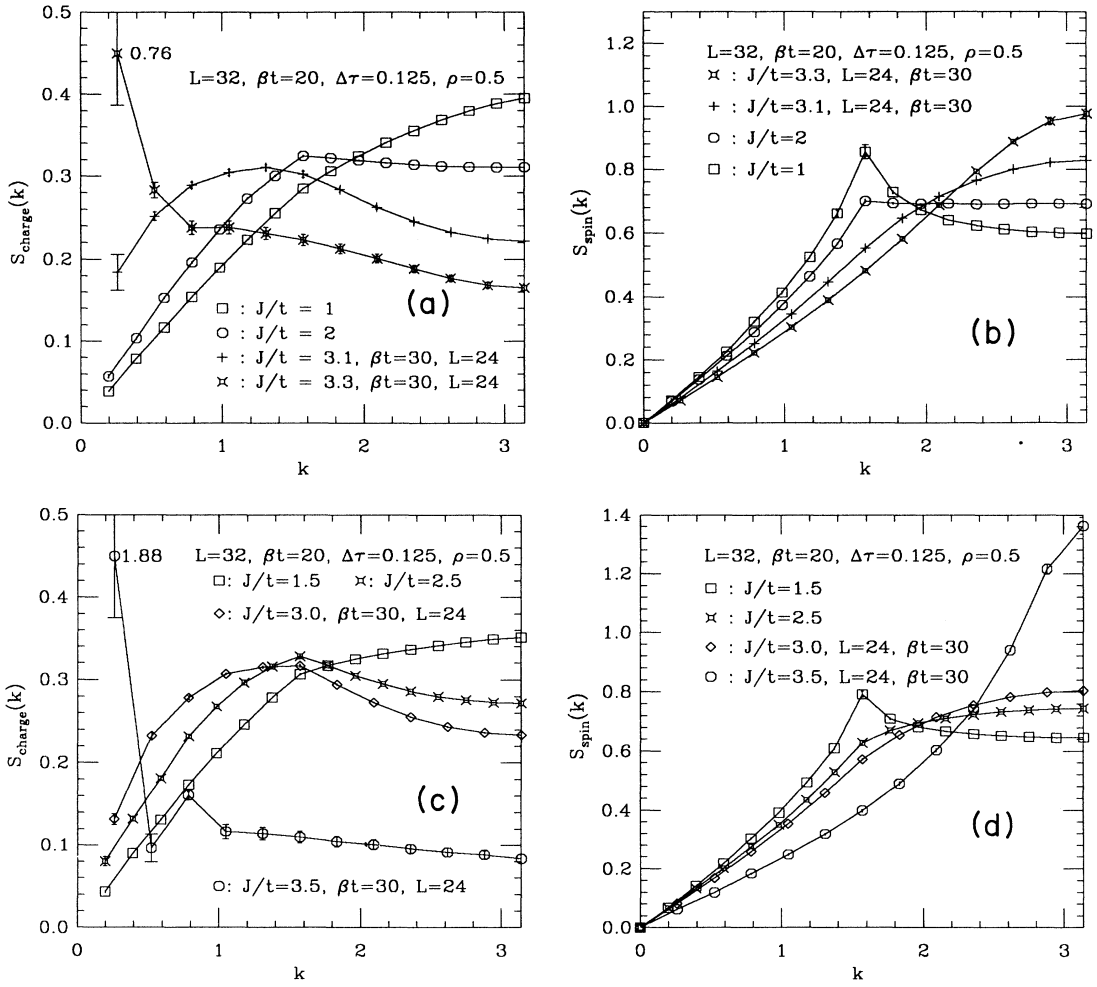

FIG. 7. (a)–(d) Spin and charge structure factors of the t-J model at quarter band filling, and values of J/t ranging from $J/t=1$ to 3.5. For each value of J/t, the temperature was chosen low enough so as to get a good approximation of the ground-state spin and charge structure. The x axis (wave vectors) covers half the Brillouin zone and for $\rho=0.5$, one has $2k_F=\pi/2$ and $4k_F=\pi$.

7(c)]. The first clear cusp at $2k_F$ in the charge structure factor may be seen at $J/t=2$ [Fig. 7(a)] and one may guess it at $J/t=1.5$ [Fig. 7(c)]. As a consequence of this pairing, the $2k_F$ spin peak is reduced in magnitude as J/t is enhanced [Figs. 7(b) and 7(d)]. As mentioned above, for values of $J/t \leq 2$ the pairing correlations, however, never dominate the long-range order. As in the repulsive Hubbard model, the spin-spin correlations for values of $J/t<2$ seem to dominate the *long-range* order.

The $2k_F$ cusp in the charge structure factor survives when J/t is enhanced from $J/t=2.0$ to 3.0 [Figs. 7(a) and 7(c)]. The $4k_F$ charge cusp is, however, not apparent any more. As mentioned above, it is the pairing of charges on adjacent sites which destroys the $4k_F$ charge cusp and creates a $2k_F$ one. The enhancement of the charge structure factor at low values of the wave vector may equally be explained by this pairing. As J/t is enhanced in the above range, the $2k_F$ cusp in the spin structure factor is smeared out and a maximum develops at $k=\pi$ [Figs. 7(b) and 7(d)]. This maximum at $k=\pi$ reflects short-range antiferromagnetic correlations. At $J/t=3.1$ [Figs. 7(a) and 7(b)], both the spin and charge structure factors are relatively smooth functions of k and thus only short-range charge and spin correlations are to be expected. For this value of J/t, the spin structure factor may be compared to that of a gas of bound pairs (i.e., a pair of electrons on adjacent sites in a singlet spin state) which takes the form $S_{\text{spin}}(k)=0.5[1-\cos(k)]$, where the lattice constant is set to 1. This form qualitatively reproduces the Monte Carlo (MC) data.

Finally, at $J/t \geq 3.3$, a peak in the charge structure factor develops at the longest wavelength ($k=2\pi/L$). This instability towards long-wavelength charge fluctuations corresponds to the onset of phase separation. As a caricature of the phase separated state, one may consider the limit $J/t \to \infty$, where the ground state consists of an island of antiferromagnetically ordered spins. As a consequence of this caricature, the ground-state energy per site is expected to be equal to $-\rho J \ln(2)$ up to corrections of order $t^2/(JL)$ and finite-size effects. The onset of the linear scaling of the energy with the density may be seen in Fig. 6. Note that in contrast to $J/t=3.5$ [Fig. 7(d)], $J/t=3.3$ [Fig. 7(b)] does not show a distinct peak in the spin structure at $k=\pi$ corresponding to the formation of island of antiferromagnetically ordered spin, although phase separation is present.

In summary, Figs. 8(a)–8(f) plot the real-space spin and charge correlations at $J/t=1$, 3.1, and 3.8. At $J/t=1$ the spin-spin correlations dominate the long-range order, and one may see a distinct $2k_F$ spin density wave [Fig. 8(a)]. On the scale of Fig. 8(a), the $4k_F$ charge density wave is, however, not apparent. At $J/t=3.8$ the ground state is fully phase separated. The spin correlations show antiferromagnetic order [Fig. 8(e)]. The charge correlations are compared to those predicted by the caricature [Fig. 8(f)]. The agreement is good. At $J/t=3.1$ [Figs. 8(c) and 8(d)], only short-range spin and charge correlations may be seen. In contrast to $J/t=1$, the next-neighbor charge-charge correlation is greater than the nearest next-neighbor one. The spin-spin correlations show strong next-neighbor antiferromagnetic correlations and no long-range order. They are compared to those of a gas of bound pairs. At $J/t=3.1$, both spin and charge correlations thus favor the existence of bound pairs.

2. $\rho=0.75$ and 0.25

Before phase separation, the charge and spin structure factors for both the low-density data, $\rho=0.25$ [Figs. 9(a)–9(d)], and the high-density data, $\rho=0.75$ [Figs. 10(a)–10(d)], show qualitatively the same behavior as for $\rho=0.5$ [Figs. 7(a)–7(d)]. In both cases, as J/t is enhanced the $2k_F$ spin cusp is smeared out and a maximum is formed at $k=\pi$. Again, for values of $J/t<2$, the charge structure factor shows a $4k_F$ as well as a $2k_F$ cusp. For values of $J/t>2$, the $4k_F$ charge cusp is not apparent any more.

It is now interesting to compare the charge structure factors of the t-V [Fig. 11(a)] and t-J models [Figs. 7(a) and 7(c)]. For small values of V/t ($V/t=0.5$), the t-V model shows a $4k_F$ charge cusp. This is comparable to the t-J model at $J/t=1$ [Fig. 7(a)]. As V/t is enhanced to $V/t=1.9$, the $4k_F$ charge cusp is smeared out, but no $2k_F$ cusp or further structure is formed as in the t-J model. In real space [Fig. 11(b)], and in contrast to the t-J model [Fig. 8(d)], one may see that in the t-V model the next-neighbor charge-charge correlation is always smaller than the next nearest-neighbor one. The discrepancy of the charge structure factors between the t-J and t-V models may be explained by the lack of mechanism in the t-V model of forming energetically favorable bound pairs.

B. Phase separation

When comparing the MC data for the three considered densities (Figs. 7–10), one may see that in contrast to the t-V model (2) model, the onset of phase separation in the t-J model is density dependent. At $\rho=0.25$, $J/t=3.1$ [Fig. 9(a)] the MC data favors a phase separated state. However at $J/t=3.1$, $\rho=0.5$ [Fig. 7(a)] phase separation is not present. For the latter filling, $J/t=3.3$ shows phase separation [Fig. 7(a)], however, $\rho=0.75$, $J/t=3.3$ [Fig. 10(c)] shows no phase separation. Thus, as the coupling J/t is lowered, the breakdown of the phase-separated state first occurs at high densities. As mentioned above, the onset of phase separation and the formation of an antiferromagnetic island of spins do not necessarily occur simultaneously. This feature is especially flagrant at low densities. At $\rho=0.25$, $J/t=3.1$ and 3.4 [Figs. 9(c) and 9(d)] the charge structure factors show phase separation, but the spin structure factors show no peak at $k=\pi$. The real-space charge and spin correlations for $\rho=0.25$, $J/t=3.4$ are plotted in Figs. 12(a) and 12(b). The spin-spin correlations compare very well to those of a gas of bound pairs and the charge-charge correlations show phase separation. Thus, when phase separation first occurs at low densities, the particle-rich phase is not a Heisenberg chain but a gas of bound pairs. At $\rho=0.25$, the formations of the antiferromagnetically ordered island of spins occurs at $J/t \sim 3.5$. In contrast, at $\rho=0.75$, phase separation and

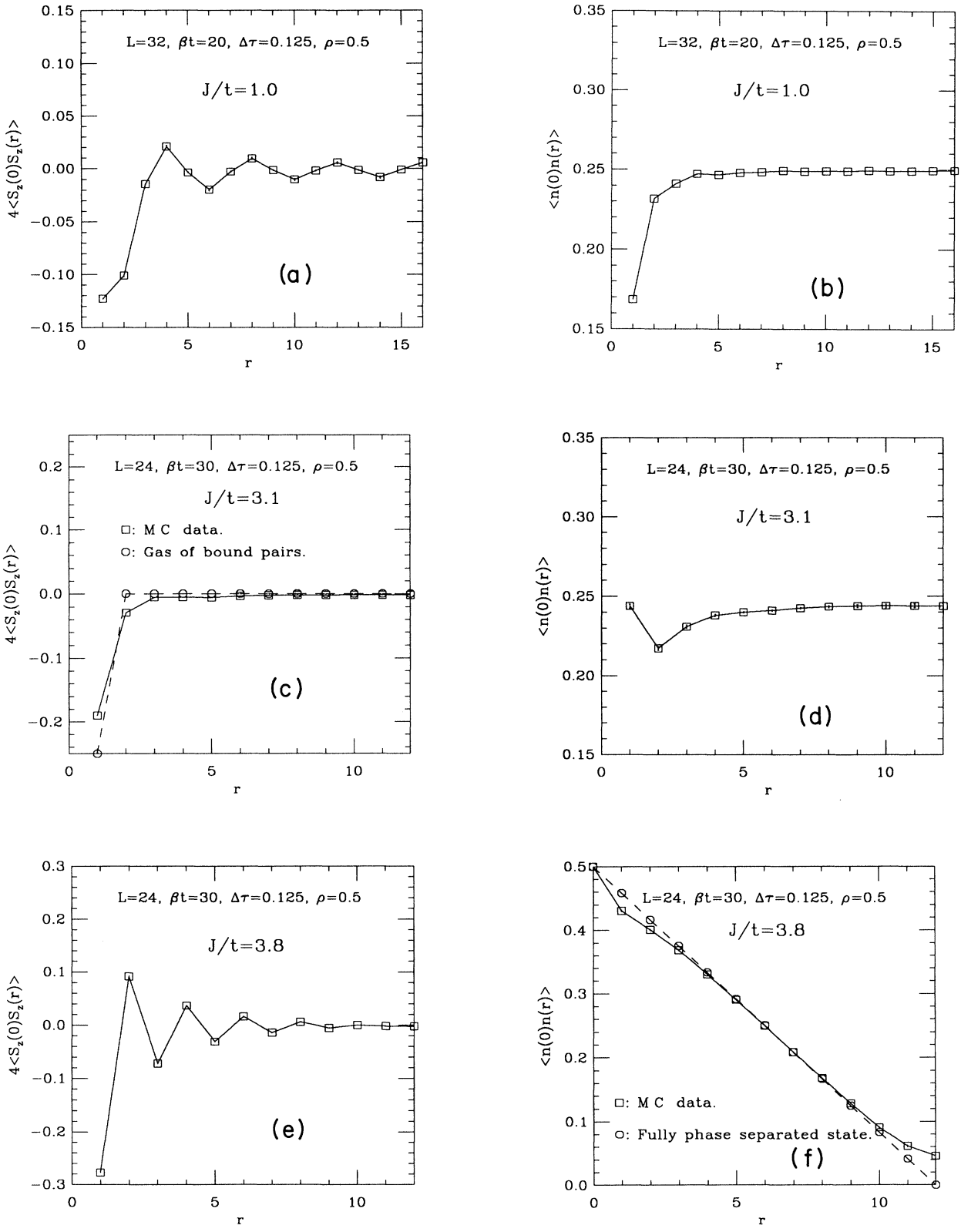

FIG. 8. (a)–(f) Real-space spin-spin and charge-charge correlations at quarter band filling and for $J/t=1$, 3.1, and 3.8. The Monte Carlo data for real-space charge-charge correlations at $J/t=3.8$ are compared to that of the fully phase separated state. The spin-spin correlations at $J/t=3.1$ are compared to those of a gas of bound pairs.

the formation of an antiferromagnetic island of spins occur simultaneously at $J/t \sim 3.5$.

In order to get more precise information on the values of J_c/t at which phase separation occurs, we have carried out a finite-size scaling study of the quantity

$$X(L)=\frac{S_{\text{charge}}(2\pi/L)}{S^{c}_{\text{charge}}(2\pi/L)} . \tag{14}$$

In the above equation, S^{c}_{charge} denotes the charge structure factor of the fully phase separated state in which the hole-rich phase consists of all holes. $X(L)$ is thus a normalized measure of the long-wavelength charge fluctuations. $X=1$ denotes the fully phase separated state $0<X<1$, a phase separated state where the particle-rich phase has $\rho<1$, and $X=0$ a uniform charge distribution (i.e., no phase separation). Here $X=X(L\rightarrow\infty)$. Figs. 13(a) and 13(b) plot $X(L)$ for the t-V model (2) as a function of V/t; $L=16,24,32$, and $\rho=0.5,0.25$. Note that the t-V model has particle-hole symmetry so that the values of $X(L)$ for $\rho=0.25$ and 0.75 are identical. As mentioned in the Introduction, the t-V model shows a first-order phase transition to a phase separated state at $V/t=2$ and for all values of the band filling. In the thermodynamic limit and at zero temperature, one thus expects X to show a discontinuity at $V/t=2$ ($X=0$ for $V/t<2$ and $X=1$ for $V/t>2$). The onset of this singularity may be seen in the Monte Carlo data since $X(L)$ scales to zero with the lattice size for $V/t<2$ and scales to one for $V/t>2$ [Figs. 13(a) and 13(b)].

Figures 14(a) and 14(b) show the finite-size scaling of $X(L)$ for the t-J model at $\rho=0.25$ and 0.75. In contrast

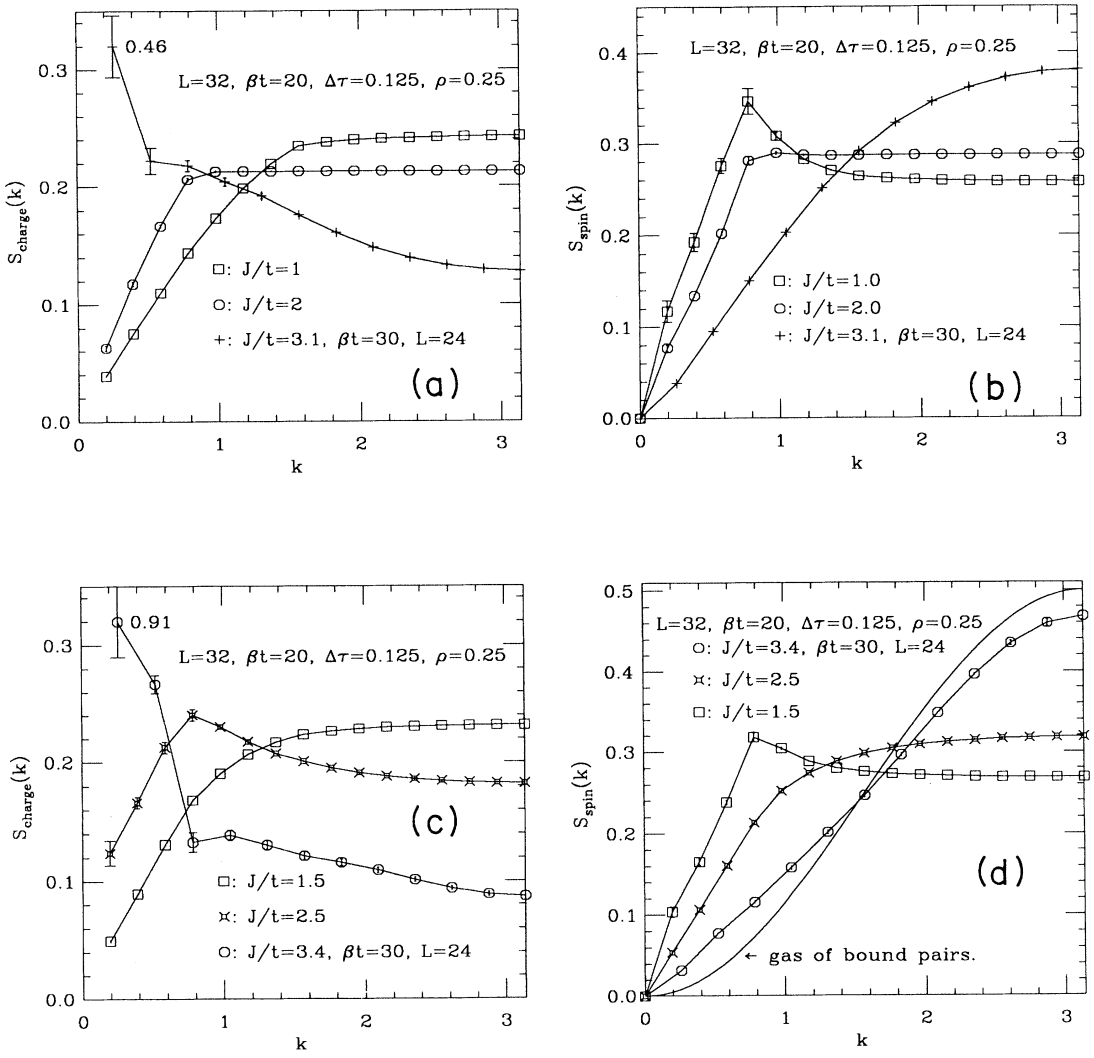

FIG. 9. (a)–(d) Spin and charge structure factors of the t-J model at $\rho=0.25$, and values of J/t ranging from $J/t=1$ to 3.4. For this filling, one has $2k_F=\pi/4$ and $4k_F=\pi/2$. In (d) we have included the spin structure factor of a gas of bound pairs. It is to be compared with the Monte Carlo data for $J/t=3.4$.

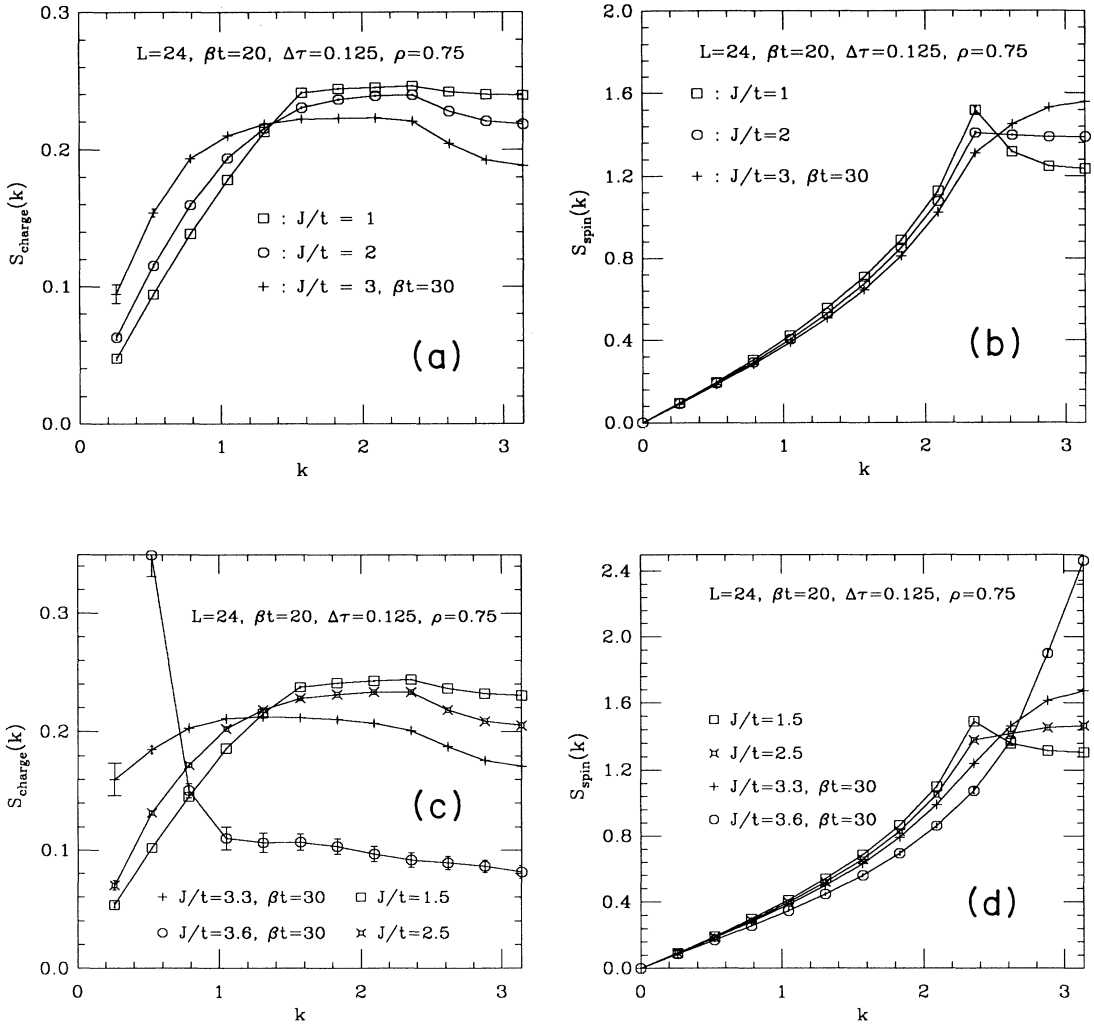

FIG. 10. (a)–(d) Spin and charge structure factors of the t-J model at $\rho=0.75$, and values of J/t ranging from $J/t=1$ to 3.25. For this filling, one has $2k_F=3\pi/4$ and $2\pi-4k_F=\pi/2$.

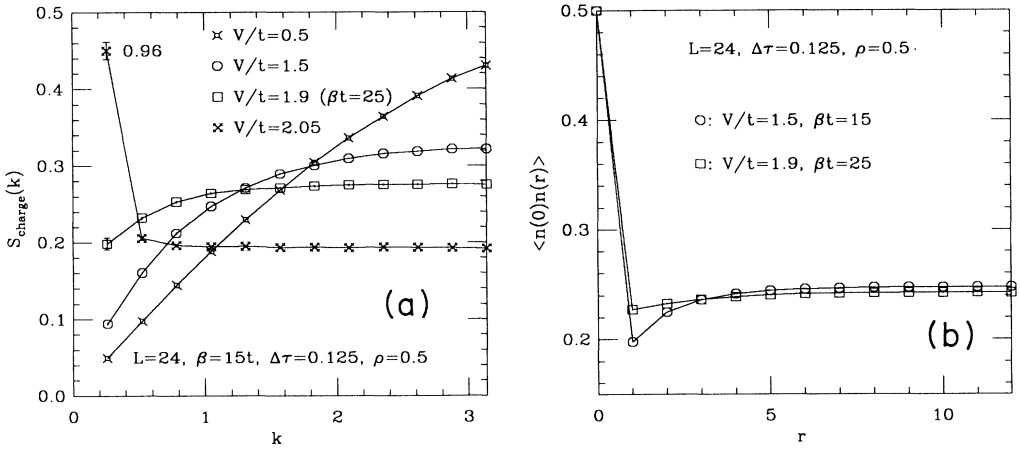

FIG. 11. (a) Charge structure factor for the t-V model at quarter band filling and $V/t=0.5$, 1.5, 1.9, 2.05. For this filling one has $4k_F=\pi$. (b) Real-space charge-charge correlations for t-V model at quarter band filling and $V/t=1.5$ and 1.9. In comparison with the t-J model (Fig. 8), the next-neighbor charge-charge correlation is always smaller than the second next-neighbor one.

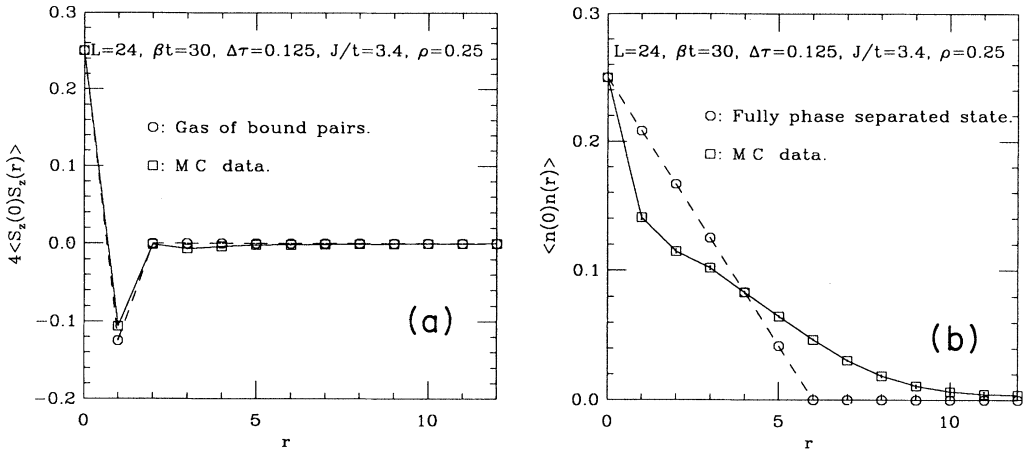

FIG. 12. Monte Carlo data for the (a) real-space charge-charge and (b) spin-spin correlations for the t-J model at $\rho=0.25$ and $J/t=3.4$. The real space charge-charge correlations are compared to those of the fully phase separated state and the spin-spin correlations to those of a gas of bound pairs.

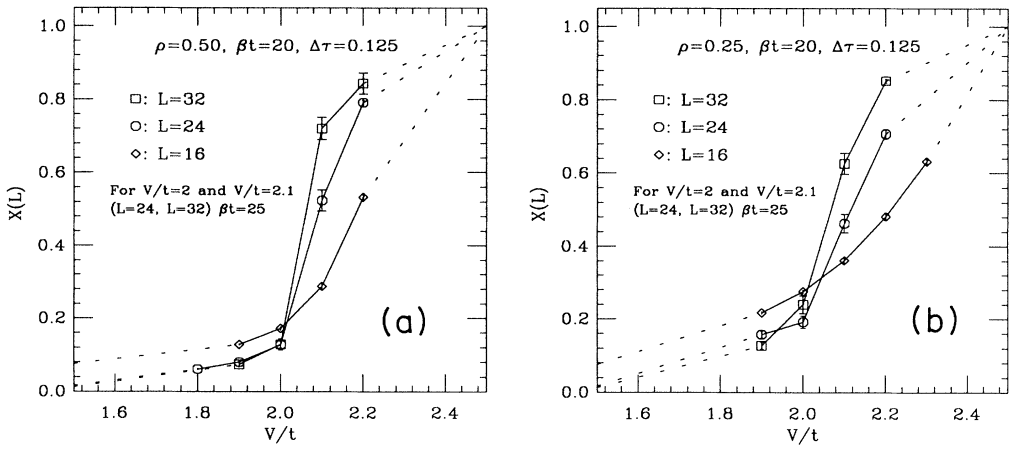

FIG. 13. Finite-size scaling of the quantity $X(L)$ (14) for the t-V model at (a) $\rho=0.25$ and (b) $\rho=0.75$. Note that the t-V model has particle-hole symmetry so that the values of $X(L)$ for $\rho=0.25$ and 0.75 are identical.

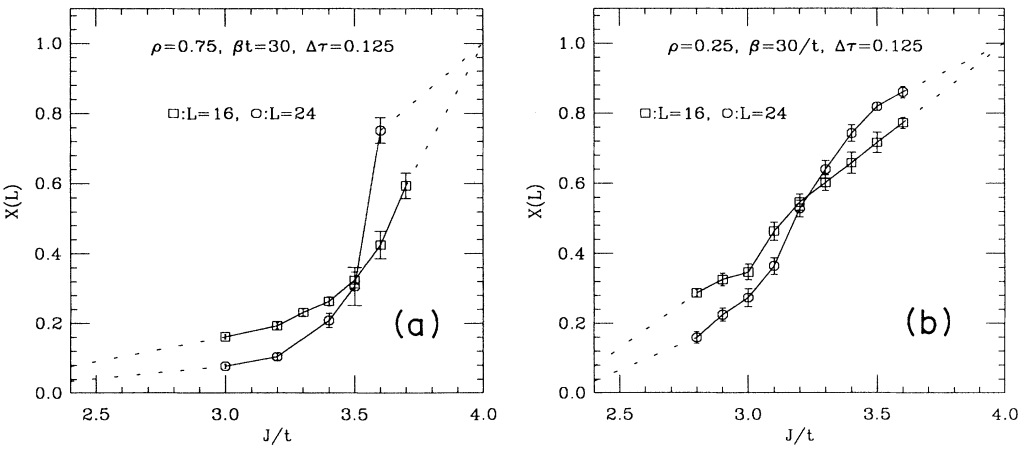

FIG. 14. Finite-size scaling of the quantity $X(L)$ (14) for the t-J model at (a) $\rho=25$ and (b) $\rho=75$. The value of J/t where the finite-size scaling of $X(L)$ is reversed yields the upper bound to the value of J/t at which phase separation occurs.

to the t-V model, the finite-size scaling of $X(L)$ for the t-J model shows a large density dependency. Our interpretation of the Monte Carlo results for the t-V model relies on the fact that in the thermodynamic limit and at zero temperature, the model shows a uniform charge distribution ($X=0$) for $V/t<2$ and a totally phase separated state for ($X=1$) $V/t>2$. This picture, however, does not hold for the t-J model, since as mentioned above at low densities one may find phase-separated states where the particle-rich phase is a gas of bound pairs. Provided that those states survive in the thermodynamic limit, the quantity X may take intermediate values between zero and one and the MC data merely provides an upper bound to J_c/t. At high density ($\rho=0.75$), $X(L)$ shows qualitatively the same behavior for both the t-J and t-V models. This reflects the fact that at this filling phase separation and the formation of an antiferromagnetic island of spins occur simultaneously. The MC data thus yields $J_c/t<3.5\pm0.1$ for $\rho=0.75$ and $J_c/t<3.25\pm0.15$ for $\rho=0.25$. This upper bound compares well with the exact diagonalization results of Ogata *et al.*[32] They find that the compressibility diverges at $J_c\sim3.5$ for $\rho=0.75$ and at $J_c/t\sim3.0$ at $\rho=0.25$.

There are a number of mechanisms in which the fully phase separated state may break down. Let us denote the value of J/t at which this happens by $J_c^{(1)}/t$. From our Monte Carlo data, one may give a lower bound for $J_c^{(1)}/t$: $J_c^{(1)}/t>3.5\pm0.1$. Let us first estimate $J_c^{(1)}/t$ by using an argument proposed by Emery, Kivelson, and Lin[33] for phase separation in the two-dimensional t-J model. The cost in energy to remove one spin from the antiferromagnetic phase is of $-J\ln(2)$, and the gain when inserting it in the hole phase is $-2t$. The fully phase separated state will thus be unstable to the transfer of one electron if $J/t<2.88$. Let us now remove a pair of spins from the antiferromagnetic phase. In the hole phase, the pair of electrons may form a singlet state on adjacent sites (i.e., a bound pair), thus minimizing the Heisenberg energy to $-J$. Taking into account the hopping term within second-order perturbation theory yields an instability of the fully phase separated state at $J/t=3.22$. As J/t is decreased, there will thus be an instability to bound pairs before single particles. Provided that the instability towards three (or more) particle clusters occurs at values of $J/t<3.22$, the Emery argument predicts $J_c^{(1)}/t=3.22$, which stands in contradiction to the above lower bound.

Another mechanism that destroys the fully phase separated state consists of holes penetrating into the particle-rich phase. Putting a pair of holes in the antiferromagnetic state destroys two antiferromagnetic bonds. This loss in energy may be compensated by a gain in kinetic energy for the holes. The value of $J_c^{(1)}/t$ corresponding to this mechanism has been evaluated numerically by Ogata *et al.*[32] and yields $J_c^{(1)}/t\sim3.5$, which is consistent with the preceding lower bound. Furthermore, the above value of $J_c^{(1)}/t$ coincides with the breakdown of the antiferromagnetic island of spins for the three considered band fillings.

C. Critical exponents and pairing correlations

From the static charge and spin structure factors, one may calculate the charge and spin exponents and thus K_ρ (13). Consider the quantity

$$b_{\text{charge,spin}}(k,L/2)\equiv 2S_{\text{charge,spin}}(k) - S_{\text{charge,spin}}(k+2\pi/L) - S_{\text{charge,spin}}(k-2\pi/L)\,. \quad (15)$$

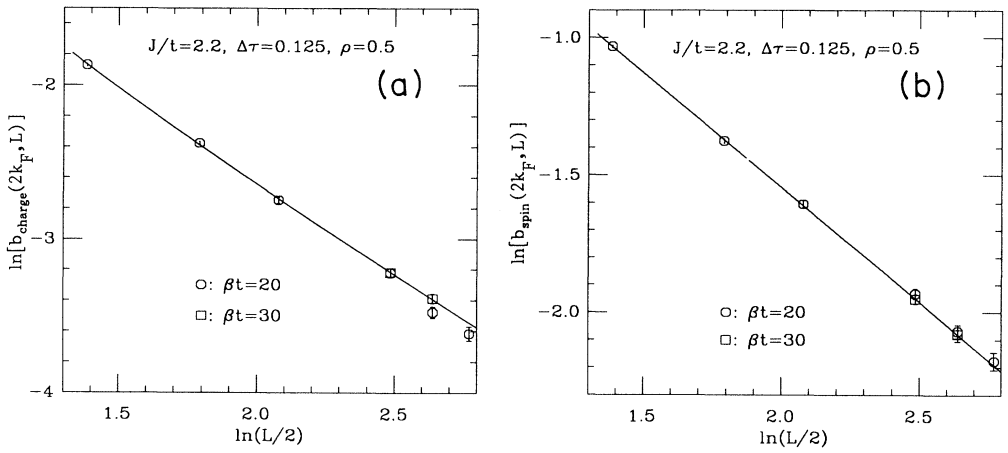

FIG. 15. Finite-size scaling of the quantity (a) $b_{\text{charge}}(2k_F,L/2)$ and (b) $b_{\text{spin}}(2k_F,L/2)$ as defined in Eq. (15), at quarter band filling and at $J/t=2.2$. We have considered two temperatures $\beta t=30$ and 20 and lattice sizes ranging from $L=8$ to 32. For lattices up to $L=24$, $\beta t=20$ is high enough so to get the ground-state properties. This may be seen by comparing the $\beta t=30$ and 20 data for the lattice size $L=24$. On the other hand, the lattice size $L=28$ requires a lower temperature. In order to extract the critical exponent, we have considered the $\beta t=20$ data for lattices up to $L=16$ and the $\beta t=30$ data for the lattice sizes $L=24$ and 28. At $L=32$ we were not able to reach sufficiently low temperatures with the required accuracy. The least-squares fit to the form (17) is plotted and yields $K_\rho^{\text{charge}}=0.93\pm0.2$ and $K_\rho^{\text{spin}}=0.84\pm0.15$. As mentioned in the text, the critical exponent are very sensitive to temperature. Considering only the $\beta t=20$ data for the charge exponent yields $K_\rho^{\text{charge}}=1.32\pm0.2$.

The spin and charge correlations between the two farthest points on the lattice may then be written as

$$\langle (n_{0,\uparrow} \pm n_{0,\downarrow})(n_{L/2,\uparrow} \pm n_{L/2,\downarrow}) \rangle = \frac{1}{4L} \sum_k e^{ikL/2} b_{\text{charge,spin}}(k, L/2) . \quad (16)$$

Assuming that the quantity $b(k, L/2)$ scales as $(L/2)^{\gamma_k}$, the long-range correlations will be dominated by the k value for which γ_k is maximal. The k values that come into consideration are those for which the structure factor shows a cusp (i.e., a nonanalytical point). We have tested the above procedure on free spinless electrons [$V=0$ in the t-V model (2)] at quarter band filling and at $\beta t = 10$. (Note that for free spinless electrons, the above temperature is low enough so as to see the ground-state properties of lattices up to 32 sites.) From our finite-size analysis, we obtained -2.03 ± 0.04 for the $4k_F$ charge exponent and the exact result is -2.

We have measured the $2k_F$ charge and spin critical exponents for the t-J model at $J/t = 2.2$ and at quarter band filling [Figs. 15(a) and 15(b)]. Applying the above method to the t-J model is more difficult than for free spinless fermions since one has to take into account the logarithmic corrections to the correlation functions (13). This may be done by fitting $b_{\text{charge,spin}}(2k_F, L/2)$ to the form

$$b_{\text{charge,spin}}(2k_F, L/2) = a - K_\rho^{\text{charge,spin}} \ln(L/2) + \gamma \ln[\ln(L/2)] . \quad (17)$$

Practically, the last term on the right-hand side of (17) has as a consequence the blowing up the error bars on $K_\rho^{\text{charge,spin}}$ and rendering the critical exponents extremely sensitive to temperature. In order to deal with the temperature effects, we have adjusted the temperature to the lattice size so as to get the ground-state properties for each lattice size. Fitting the so obtained data to the form (17) yields the following for the $2k_F$ charge and spin exponents: $K_\rho^{\text{charge}} = 0.93 \pm 0.2$ and $K_\rho^{\text{spin}} = 0.84 \pm 0.15$ ($J/t = 2.2$, $\rho = 0.5$). If the t-J model at $J/t = 2.2$ belongs

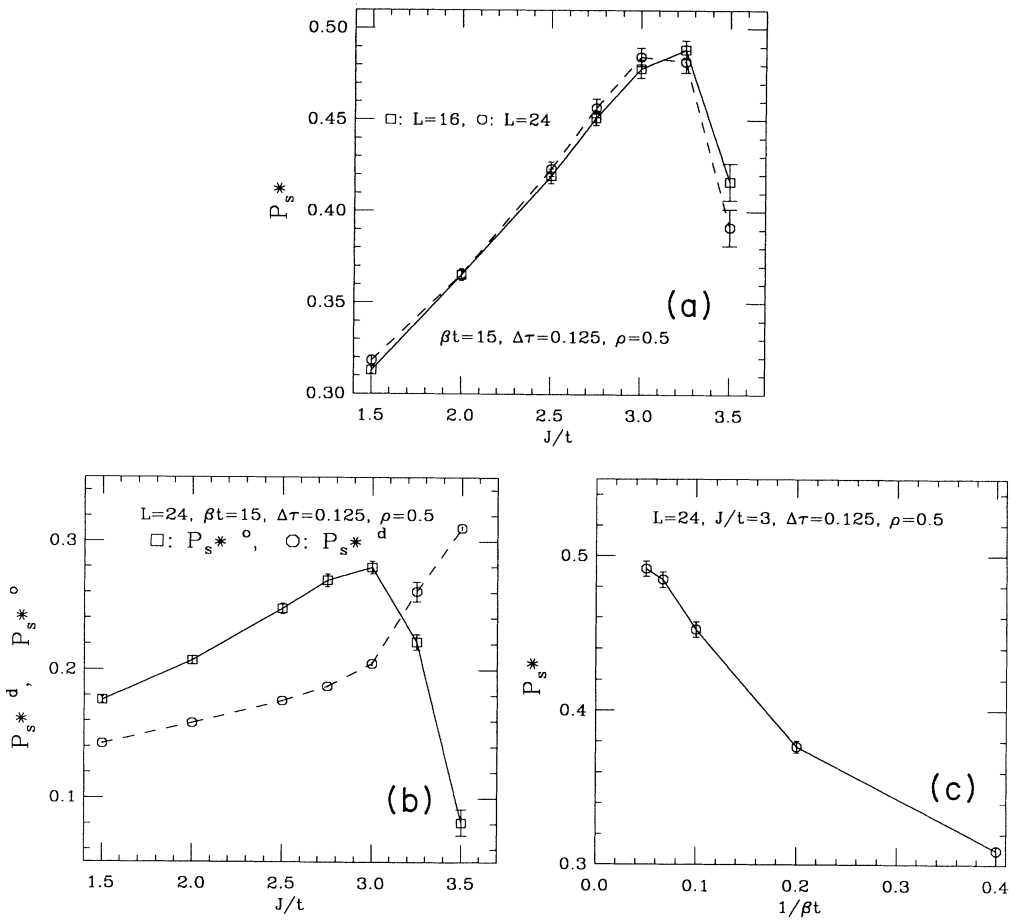

FIG. 16. (a) Equal-time pairing correlations in the extended s-wave channel as a function of J/t and at quarter band filling. (b) The equal-time pairing correlations in the extended s-wave channel are decomposed in a diagonal (octagons) and off-diagonal part (squares) as described in the text. As may be seen, it is the off-diagonal contribution that is responsible for the drop of pairing correlations as one enters the phase separated state. (c) Temperature dependence of the pairing correlations.

to the same universality class as that for $J/t=2$ (see arguments in Ref. 32), Eq. (13) requires $K_\rho^{\text{spin}}=K_\rho^{\text{charge}}=K_\rho$, which (within the error bars) is consistent with the MC data.

Within the Luttinger liquid theory, K_ρ is related to the compressibility κ through[8]

$$\frac{1}{\rho^2\kappa}=\frac{\pi}{2}\frac{v_c}{K_\rho} , \tag{18}$$

where v_c is the charge velocity. Using the above equation, Ogata *et al.*[32] have derived K_ρ. Their results compare favorably with the MC data. They equally find a region before phase separation where $K_\rho>1$, so that the pairing correlations are expected to dominate the long-range order (13).

We have measured equal-time pairing correlations in the extended s-wave channel

$$P_{s*}=\langle \Delta_{s*}^\dagger \Delta_{s*} \rangle , \tag{19}$$

where

$$\Delta_{s*}=\sqrt{2/L}\sum_k \cos(k) c_{k,\uparrow} c_{-k,\downarrow} .$$

Figure 16(a) plots P_{s*} at quarter band filling as a function of the coupling $J/t, \beta t=15$, $L=16$ and 24. For both lattice sizes, and before phase separation, P_{s*} is very much enhanced by growing values of J/t and shows a maximum at approximately $J/t=3$. In the phase-separated state P_{s*} drops. It is interesting to note that the interaction term of the t-J model may be written as

$$J\sum_i (\mathbf{S}_i\cdot\mathbf{S}_{i+1}-\tfrac{1}{4}n_i n_{i+1})=-J\sum_i b_i^\dagger b_i . \tag{20}$$

Due to the minus sign appearing on the right-hand side of the above equation, one may see that for growing values of J/t bound pairs become energetically increasingly favorable. In order to see this one may split P_{s*} into a diagonal term

$$P_{s*}^d=\frac{1}{L}\sum_i \langle b_i^\dagger b_i \rangle$$

and into an off-diagonal term

$$P_{s*}^0=\frac{1}{L}\sum_{\substack{i,j \\ (i\neq j)}} \langle b_j^\dagger b_i \rangle .$$

The diagonal term merely counts the number of bound pairs, while the off-diagonal term is a measure of the correlation between pairs. Figure 16(b) plots both terms separately for the 24-site lattice. Before phase separation, both P_{s*}^d and P_{s*}^o grow with increasing values of J/t. As one enters the phase-separated state, the number of bound pairs (P_{s*}^d) still increases, while P_{s*}^o is drastically suppressed. Finally, as the temperature is lowered, P_{s*} increases [Fig. 16(c)].

IV. CONCLUSIONS

In conclusion, let us draw a qualitative phase diagram of the one-dimensional t-J model. The charge and spin structure factors before phase separation show qualitatively the same structure for the three considered densities ($\rho=0.25$, 0.5, and 0.75). At small values of J/t, the model shows a $U/t\to\infty$ Hubbard-like character, namely a $4k_F$ charge cusp, a $2k_F$ spin cusp, and the domination of the spin-spin correlations at large distances. As J/t is enhanced in the range $0<J/t<J_c/t$, the $2k_F$ spin cusp is smeared out and the spin structure factor develops a maximum at $k=\pi$. As for the charge structure factor, when J/t is enhanced in the range $0<J/t<2$, the $4k_F$ charge cusp is smeared out and one at $2k_F$ is formed. For values of $J/t\geq 2$ only the $2k_F$ cusp in the charge structure factor is apparent. Those changes in the spin and charge structure factors as a function of the coupling J/t may be seen as a consequence of the gradual pairing of charges on adjacent sites as J/t is enhanced. Further information on the formation of pairing correlations was obtained by measuring the pairing correlations in the extended s-wave channel. The MC data show that they are very much enhanced by growing values of J/t and before phase separation. In contrast, the t-V model (2) shows no such pairing mechanism.

We have measured the $2k_F$ charge (K_ρ^{charge}) and spin (K_ρ^{spin}) critical exponents at $J/t=2.2$ and at quarter band filling. Provided that the model scales to the same fix point as for $J/t=2$ (see arguments in Ref. 32), one expects $K_\rho^{\text{charge}}=K_\rho^{\text{spin}}\equiv K_\rho$ (13), which is compatible with our error bars. In terms of K_ρ, the MC data thus support that K_ρ is enhanced by growing values of J/t. One equally expects K_ρ to take values greater than 1 (i.e., pairing correlation functions dominate the long-range order) within a region $2<J/t<J_c/t$. Those expectations are in agreement with the exact diagonalization results of Ogata *et al.*[32]

Phase separation in the t-J model occurs in a very subtle way. In contrast to the t-V model, J_c/t is density dependent: as J/t is reduced, the phase-separated state first breaks down at large densities. Furthermore, the nature of the particle-rich phase for low densities (e.g., $\rho=0.25$) is not restricted to a Heisenberg chain, since for values of J/t within the range $J_c/t<J/t\lesssim 3.5$ it takes the form of a gas of bound pairs. The MC data provide an upper bound to J_c/t and yields $J_c/t<3.5\pm0.1$ for $\rho=0.75$ and $J_c/t<3.25\pm0.15$ for $\rho=0.25$, which compare well with the results of Ogata *et al.*[32] In contrast to the two-dimensional t-J model, the fully phase-separated state does not break down through the diffusion of pairs of particles in the hole-rich phase,[33] but through the diffusion of pairs of holes in the particle-rich phase.

ACKNOWLEDGMENTS

This work has been supported in part by a grant from the Zentenarfonds of the ETHZ. We wish to thank Professor T. M. Rice and M. Ogata for very helpful discussions and for giving us ideas on the overall structure of the phase diagram of the one-dimensional *t-J* model. We are also grateful for many discussions with P. A. Bares, G. Blatter, B. Gölzer, M. Luchini, S. Sorella, W. Putikka, and X. Zotos.

[1]P. W. Anderson, Science **235**, 1196 (1987).
[2]F. C. Zhang and T. M. Rice, Phys. Rev. B **37**, 3759 (1988).
[3]J. E. Hirsch, Phys. Rev. Lett. **54**, 1317 (1985).
[4]E. H. Lieb and F. Y. Wu, Phys. Rev. Lett. **20**, 1445 (1968).
[5]S. Sorella, A. Parola, M. Parrinello, and E. Tosatti, Europhys. Lett. **12**, 721 (1990); A. Parola and S. Sorella, Phys. Rev. Lett. **64**, 1831 (1990).
[6]M. Ogata and H. Shiba, Phys. Rev. B **41**, 2326 (1990).
[7]H. Frahm and V. E. Korepin, Phys. Rev. B **43**, 5653 (1991).
[8]H. J. Schulz, Int. J. Mod. Phys. B **5**, 57 (1991).
[9]B. Sutherland, Phys. Rev. B **12**, 3795 (1975).
[10]P. Schlottmann, Phys. Rev. B **36**, 5177 (1987).
[11]P. A. Bares, G. Blatter, Phys. Rev. Lett. **64**, 2567 (1990).
[12]N. Kawakami and S. K. Yang, Phys. Rev. Lett. **65**, 2309 (1990).
[13]J. E. Hirsch, D. J. Scalapino, R. L. Sugar, and R. Blankenbecler, Phys. Rev. Lett. **47**, 1628 (1981); J. E. Hirsch, R. L. Sugar, D. J. Scalapino, and R. Blankenbecler, Phys. Rev. B **26**, 5033 (1982).
[14]H. de Raedt and A. Lagendijk, Phys. Rev. Lett. **46**, 77 (1981); J. Stat. Phys. **27**, 731 (1982).
[15]M. Suzuki, Phys. Rev. B **31**, 2975 (1985).
[16]H. Betsuyaku, Prog. Theor. Phys. **75**, 774 (1986).
[17]I. Morgenstern and D. Würtz, Phys. Rev. B **32**, 532 (1985).
[18]M. Imada and Y. Hatasugai, J. Phys. Soc. Jpn. **58**, 3752 (1989); M. Imada, in *Proceedings of the International Workshop on Quantum Simulations of Condensed Matter Phenomena, Los Alamos, 1989,* edited by F. D. Doll and J. E. Gubernatis (World Scientific, Singapore, 1989), p. 127.
[19]M. Suzuki, Prog. Theor. Phys. **56**, 1454 (1976).
[20]H. F. Trotter, Proc. Am. Math. Soc. **10**, 545 (1959).
[21]C. N. Yang and C. P. Yang, Phys. Rev. **150**, 321 (1966); **150**, 327 (1966).
[22]F. D. M. Haldane, Phys. Rev. Lett. **46**, 1358 (1980).
[23]A. Luther and I. Peschel, Phys. Rev. B **12**, 3908 (1975).
[24]F. F. Assaad and D. Würtz, Helv. Phys. Acta **63**, 841 (1990).
[25]*Quantum Monte Carlo Methods,* edited by M. Suzuki (Springer-Verlag, Heidelburg, 1987); *Monte Carlo Methods in Quantum Problems,* edited by M. Kalos (Reidel, Dordrecht, 1984).
[26]S. Sorella, E. Tosatti, S. Baroni, R. Car, and M. Parrinello, Int. J. Mod. Phys. B **1**, 993 (1988); S. Sorella, S. Baroni, R. Car, and M. Parrinello, Europhys. Lett. **8**, 663 (1989); F. F. Assaad and D. Würtz, Z. Phys. B **80**, 325 (1990); F. F. Assaad, Helv. Phys. Acta **63**, 580 (1990).
[27]S. R. White, D. J. Scalapino, R. L. Sugar, E. Y. Loh, J. E. Gubarnatis, and R. T. Scalettar, Phys. Rev. B **40**, 506 (1989).
[28]M. Barma and B. S. Shastry, Phys. Lett. **61A**, 15 (1977).
[29]M. Barma and B. S. Shastry, Phys. Rev. B **18**, 3351 (1978).
[30]R. J. Baxter, *Exactly Solved Models in Statistical Mechanics* (Academic, New York, 1982).
[31]B. Gölzer, J. Phys. A **22**, L25 (1989).
[32]M. Ogata, M. U. Luchini, S. Sorella, and F. F. Assaad, Phys. Rev. Lett. **66**, 2388 (1991).
[33]V. J. Emery, S. A. Kivelson, and H. Q. Lin, Phys. Rev. Lett. **64**, 475 (1990).